Chitosan-functionalized sodium alginate-based electrospun nanofiber membrane for As (III) removal from aqueous solution

Md Eman Talukder [a,b,c,1], Md. Nahid Pervez [d,1], Wang Jianming c, Ziwei Gao [e], George K. Stylios [f], Mohammad Mahbubul Hassan [g], Hongchen Song [a,b,c,*], Vincenzo Naddeo [d,**]

a *Shenzhen Institute of Advanced Technology, Chinese Academy of Sciences, Shenzhen 518055, China* b *University of Chinese Academy of Sciences, Beijing 100049, China* c *Guangzhou Institute of Advanced Technology, Guangzhou 511458, China* d *Sanitary Environmental Engineering Division (SEED), Department of Civil Engineering, University of Salerno, via Giovanni Paolo II 132, 84084 Fisciano, SA, Italy* e *School of Ecological and Environmental Sciences, East China Normal University, Shanghai 200241, China* f *Research Institute for Flexible Materials, School of Textiles and Design, Heriot-Watt University, Galashiels TD1 3HF, UK* g *Bioproduct and Fiber Technology Team, AgResearch Limited, 1365 Springs Road, Lincoln, Christchurch 7674, New Zealand*

Abstract:

Environment-friendly chitosan-modified-poly(vinyl alcohol) or (PVA)/sodium alginate (SA) electrospun nanofiber membrane (ENM) adsorbent was prepared for the removal of As(III) from an aqueous solution. The chitosan (CS)-functionalized-PVA/SA ENM (CS-f-PVA/SA) was characterized by scanning electron microscopy (SEM), Fourier transform infrared spectroscopy (FTIR), thermogravimetric analysis (TGA), and X-Ray diffraction (XRD). The CS-f-PVA/SA ENM showed the maximum As (III) adsorption capacity at neutral pH (540.40 mg g□ 1). The adsorption experiments were conducted by varying the initial pH of the arsenic solutions and also in the presence of different coexisting anions, such Cl- and F-, SO42□ , and PO43□ . Moreover, the kinetic studies were performed to depict the rate of As(III) sorption onto CS-f-PVA/SA ENM. The As(III) adsorption reached equilibrium within 90 min, which well fitted to the pseudo-second-order kinetic model. The initial pH of arsenic solutions greatly affected the adsorption efficiency but the presence of competing anions in arsenic solutions showed a moderate effect on the arsenic adsorption. The FTIR and XRD analyses suggest that–NH2, –OH, and C–O functional groups of CS-f-PVA/SA ENM are responsible for As(III) uptake. The prepared CS-f-PVA/SA ENM can be easily regenerated using 0.003 M NaOH, and the As(III) removal rate was still above 90–50% after ten successive adsorption-desorption cycles. Thus, such a nanofiber-based adsorbent is quite promising for the removal of As(III) from potable water and can be beneficial in combating the current challenges of arsenic pollution.

1. Introduction

Arsenic (As) in drinking water is of particular concern because of its serious health effects. The arsenic pollution of water is a serious issue for many countries in the world, including India and Bangladesh and the presence of arsenic in drinking water causes abdominal pain,

cardiovascular disease, neurological diseases, lung infection, skin lesions, and cancer [1–3]. The World Health Organization (WHO) has recommended that arsenic concentration in drinking water should not exceed 10 μg L□ 1. The speciation of arsenic shows that it is present in water mainly in two states, arsenite or As(III) and arsenate or As(V), of which As(III) possess 60 times higher toxicity than As(V). Under oxidizing conditions, AS(V) predominates but under reducing conditions AS(III) predominates. Therefore, the removal of As(III) from potable water is of utmost importance but it is a challenging task [4,5]. Various technologies, including adsorption, have been tested to date, but the adsorption process is preferred over other methods because of its simplicity, high removal capacity, being economically viable, and also because it allows recovery of arsenic [6].

In recent years, the ENMs have been found as a promising adsorbent for the removal of pollutants from aqueous solutions. Electrospinning has been recognized as a tool for the production of flexible and efficient one-dimensional nanostructured membranes with a range of submicron to nano-sized nanofibers [7,8]. They show outstanding properties, such as high surface area and porosity, no agglomeration tendency, and high pollutant binding capacity [9,10]. As a natural water-soluble non-toxic polymer, SA is being widely employed to prepare electrospun nanofiber membrane due to its biodegradability, non-toxicity, high mechanical stability, and hydrophilicity [11]. However, it is quite challenging to produce pure alginate electrospun nanofiber membrane because of high surface tension, high electrical conductivity, and lack of chain entanglements in alginate in an aqueous solution [12,13]. The addition of a synthetic polymer to alginate, such as polyvinyl alcohol (PVA), has been identified as a potential pathway to enhance electro spinnability of SA. Similarly, PVA is a water-soluble non-toxic polymer, which is highly biocompatible hydrophilic polymer with good chemical and thermal stability, and electro-spinnable at various concentrations [14]. PVA/SA nanofiber formation is facilitated by establishing a hydrogen bond between PVA and SA polymers [15]. However, only a few studies have been reported that utilized sodium alginate-based electrospun nanofibers membranes as an adsorbent for arsenic removal. Wang et al. synthesized sodium alginate electrospun nanofiber membrane for methylene blue adsorption [16]. It was reported that the maximum adsorption capacity reached 2230 mg g□ 1. The high surface area and porosity of sodium alginate electrospun nanofiber membranes are also suitable for heavy metals adsorption from an aqueous solution [17,18]. A recent study carried out by Ebrahimi et al. [19] showed that the removal of Cd2+ ions by PVA/SA electrospun nanofiber membrane reached 93.163 mg g□ 1. Although previous studies have shown that sodium alginate electrospun nanofiber could be used as an adsorbent, some adjustments are required, such as SA nanofiber has high water solubility and therefore they are weakly stable in aqueous solution, but the stability of the adsorbent in water is one of the major challenges in the adsorption process. The addition of PVA to SA will make SA electro-spinnable and coating of PVA/SA nanofiber membrane with chitosan also may enhance the stability and arsenic adsorption capacity of alginate nanofiber membrane in water. Chitosan is an interesting natural cationic polysaccharide polymer because of its beneficial physicochemical properties, including solid-state structure phenomena. In the dissolved state, it can make a chain entanglement and also has various has functional groups (carboxyl and amino) [20–23]. Most importantly, its non-toxicity and biodegradability make it a suitable candidate for environmentally-friendly adsorbent applications, especially in organic pollutants removal from potable water [24–26].

Previous studies claimed that the addition of chitosan to sodium alginate-based composites showed higher thermal and mechanical stability than the same sodium alginate composites without chitosan because of the formation of strong electrostatic bonds between amino groups of chitosan and carboxyl groups of SA [27,28]. In the present work, we developed a chitosan functionalized SA/PVA electrospun nanofiber membrane as a novel adsorbent for the removal of As(III) from water. To the best of our knowledge, no published literature reported its application for the removal of pollutants from water.

2. Experimental

2.1. Materials

In this study, 98% hydrolyzed polyvinyl alcohol (PVA) was purchased from Sinopharm Chemical Reagent Co. Ltd. (China). Sodium alginate was purchased from Tianjin Damao Chemical Reagent Factory (China). Chitosan (high viscosity, 80% deacetylated, Mw~40 × 104 g mol□ 1) was purchased from Fluke Aldrich Chemical Co. Ltd. (China). Non-woven PET paper was supplied by Guocheng CO. (Wuxi, China), which was used as a collector for electrospinning. The arsenic solution containing 1000 μg mL□ 1 in 5% 1.0 mol L□ 1 nitric acid (HNO3) () was purchased from a national standard sample library (GBS-04-1714- 2019), China. Sodium hydroxide (NaOH) and acetic acid (CH3COOH) were procured from Sinopharm Chemical Reagent Co., Ltd. (Shanghai, China). All chemicals and reagents were used without further purification.

2.2. Preparation of adsorbents

The Preparation of adsorbent solution for ENM was as follows: An aqueous solution of PVA (8%) and SA (3%) (w/v) was prepared by dissolving them in water with continuous magnetic stirring at 80 ºC temperature for 3 h or until complete dissolution and a clear and uniform solution was formed [29,30]. The solution was then cooled to room temperature. Electrospinning experiments were then carried out on a MELT Electrospinning machine **(**Model M06, Foshan Lepton Precision Measurement, and Control Technology Co., Ltd, China). The blended polymer solution was loaded into 10 mL syringes with a 20 G needle. The electrospinning of the PVA/SA solution was carried out at 16 kV at a flow rate of 0.6 mL min□ 1 and the distance between the tip of the needle and the collector (nonwoven PET paper) was 15 cm [31]. After the collection of ENM from the collector, they were dried at 60 ◦C for 6 h to remove the residual solvent.

The fabricated fibrous PVA/SA ENMs were spin-coated with chitosan [32]**.** For this purpose, 1% (w/v) amount of the chitosan casting solution was applied onto the PVA/SA ENMs placed between the casting knife and the glass plate and spin-coated at a speed of 7000 rpm at room temperature. The spin-coated chitosan-functionalized PVA/SA electrospun nanomembranes (CS-f-PVA/SA ENMs) were dried for at least 24 h at 50 ºC in a drying oven to evaporate acetic acid and the residual water in the ENM. The dried CS-f-PVA/SA-ENMs were washed with distilled water until completely neutralized [33]. They were then dried again at room temperature.

2.3. Characterization

The viscosity of SA/PVA and CS-f-SA/PVA solutions was measured at 28 ºC temperature by using a rotational viscometer (NDJ-8S Digital Viscosity Meter, Movel Scientific Instrument

Co., Ltd, China). The electrical conductivity and pH of each solution were measured by pH/ conductivity meter (Shanghai INESA Scientific Instrument Co., Ltd., China). The hydrophilicity of ENMs was evaluated by contact angle measurement (Droptmete-A300 Kudos Instruments Corporation, USA). The surface morphology of the prepared ENMs was observed using a scanning electron microscope (SEM, Phenom XL, Phenom world, Netherlands) at an accelerating voltage of 5 kV. Before the SEM scanning, the top surface of ENM samples was sputter-coated with gold to prevent them from charging. The mean diameter of nanofibers was calculated using ImageJ software (National Institute of Health, USA). The functional groups of the produced nanofibers were identified using an FTIR spectrometer (IR, Interspectrum, low noise DLATGS, FTIR-920, Estonia). Few milligrams of the ENMs and potassium bromide were mixed and ground to fine powder by a mortar and pestle before being placed on the ATR crystal to get the IR spectra. The thermal stability of the samples was measured by a thermogravimetric analyzer (Model: SDTA851e, Mettler Toledo Instruments Ltd., Shanghai, China) by heating at 20 ◦C min□ 1 under a nitrogen atmosphere. XRD patterns were recorded on an XRD instrument (Mini Flex 300/600, Rigaku Corporation, Japan) at a voltage of 40 kV and 15 mA. The data were collected from 8.0◦ to 70.0◦ at a scanning speed of 1.0◦ min□ 1. The zeta potential of the ENM surface was measured by a zeta potential analyzer (Zeta Potential Measuring Instrument (Model: ZETA-PM94J2, Xiangtan Xiangyi Instrument Limited, China).

2.4. Adsorption studies

2.4.1. Effect of adsorbent dosage

The capacity of CS-f-PVA/SA ENM to remove As(III) was investigated using a batch adsorption test by varying the dosage from 0.1 to 1.0 g L□ 1. Initial As(III) concentration at neutral pH was 250 μg L□ 1. The As(III) solution containing the adsorbent was stirred on a rotary shaker at 210 rpm for 4 h at ambient temperature. After filtration via filter paper, the arsenic concentrations were determined by an inductively coupled plasma—optical emission spectrometer (ICP-OES), (Model: Optima 8000, Perkin Elmer Company, USA). The calibration curve was prepared by measuring various concentrations of standard arsenic solutions and the prepared calibration curve is provided in Fig. S1 (Supplementary Materials). The limit of detection (LOD) and limit of quantification (LOQ) for arsenic measurement by ICP-OES are 6 and 12 μg l□ 1 respectively. The R2 value was 0.981.

2.4.2. Effect of solution pH

The effect of solution pH was examined in the range of pH 2–11 and the pH of the arsenite solution was set by adding acetic acid (CH3COOH) for acidic pH and NaOH for an alkaline pH. 10 mg adsorbent was added to 10 mL of 250 μg L□ 1 As(III) solution for each arsenic adsorption experiment and the final equilibrium As(III) concentrations were measured.

2.4.3. Effect of initial concentrations of As(III) ions

The effect of the initial concentrations of As(III) ions on the equilibrium adsorption by pristine PVA/SA ENM and CS-f-PVA/SA ENM was examined. Five initial concentrations of As(III) 200, 250, 300, 350, and 400 μg L□ 1 were used and the As(III) adsorption was carried out at room temperature.

2.4.4. Adsorption kinetics and isotherm

Adsorption experiment studies were performed to investigate the As (III) binding capacity of CS-f-PVA/SA and pristine PVA/SA ENMs. 10.0 μL of 1.0 mol L□ 1 HNO3 in distilled water was added to a certain volume of As(III) stock solution (100 μg mL□ 1) and diluted to the desired concentration. The AS(III) adsorption performance of the CS-f-PVA/SA and pristine PVA/SA ENMs was investigated using a series of experiments, such as the effect of pH, contact time, and solution concentrations, etc. The equilibrium curves were prepared by carrying out As(III) adsorption at 25 ºC. For equilibrium curves, 10 mg of CS-f-PVA/SA and pristine PVA/SA ENM adsorbents were added into a 10 mL aqueous solution containing 250, 300, 350, 400, 450 μg mL□ 1 of As(III) [34]. These samples were placed in a rotary shaker at room temperature and shook at 210 rpm. Kinetic curves with contact times ranging from 0 to 200 min were prepared at an initial As(III) concentration of 250 μg mL–1at 25 ºC and 210 rpm using an appropriate adsorbent dose and pH [34–36]. For the kinetic studies, As(III) concentrations were monitored at different time (15 min, 30 min, 50 min) intervals using the ICP-OES instrument. The percentage of As(III) ions removal was calculated using (Eq. 1). %As(III)removal = C**Csubs0** □ Ce **Csubs0** × 100 (1) The equilibrium adsorption capacities of CS-f-PVA/SA and pristine PVA/SA ENMs samples were calculated and the amount of As(III) adsorbed per unit mass of adsorbent (mg), qe (mg g□ 1), was obtained by (Eq. 2), Adsorption capacity, qe = C**Csubs0** □ Ce M × V (2) Where, Csubs0 and Ce are the initial and equilibrium concentrations of arsenic (μg mL□ 1), respectively, V is the total volume (mL) of the arsenic solution, and M is the mass of the ENM adsorbent (mg).

2.4.5. Effect of coexisting anions

Additionally, five representative coexisting anions phosphate (PO43-), sulfate (SO42-), chloride (Cl-), nitrate (NO22-), silicate (SiO32-), and fluoride (F-) with concentrations ranging from 0.5 to 1.0 mM were used to investigate the effect of competing anions on As(III) adsorption. After 1 h, the samples were filtered and analyzed for As(III) measurement [37,38]. *2.5. Regeneration experiment* The regeneration of CS-f-SA/PVA ENM adsorbent was examined by adding 10 mg of adsorbent into 50 mL As(III) solutions (250 μg mL□ 1) in a glass bottle. After 5 h of agitation at 200 rpm, the adsorbent was separated, washed with distilled water, and transferred into a 50 mL glass bottle. And then, 10 mL of the 0.05 M NaOH was added and shaked for 5 h. The adsorbent was removed, washed, neutralized, and again added to the new arsenic solution, and again the adsorbent was removed, and the concentration of As(III) was measured. 10 cycles of regeneration and reuse of adsorbent were carried out for evaluating the reusability of the developed adsorbent.

3. Results and discussion

3.1. Nanofiber formation by electrospinning

In the electrospinning process, the physical properties of the polymer solution are very important as the viscosity and conductivity of the polymer solutions have the greatest impact on the shape and diameter of the formed nanofibers and ENMs [39]. We found that PVA/SA solution of 220 mPa s viscosity and electrical conductivity of 600 mS cm□ 1 produced smooth and uniform nanofiber without bead formation. The color of CS-f-PVA/SA ENM changed from white to gray color after surface coating with chitosan**.**

3.2. Morphology

Fiber morphology is an important property since it indicates the uniform nanofiber formation and porosity of the prepared membranes. Herein, we investigated our as-prepared nanofiber and membrane morphology by SEM. It was found that the combination of 10% PVA and 2% SA produced beads-free uniform nanofiber. The distributions of the diameter of nanofibers and the morphology SA/PVA ENM before and after the functionalization with chitosan are shown in Figs. 1a and 1b, respectively. The diameter of SA/PVA nanofiber increased after the coating with chitosan. The average diameter of the PVA/SA nanofibers was about 159 nm but after coating with chitosan, the diameter of the nanofibers increased to 164 nm as shown in Figs. 1c and 1d, respectively. The change in nanofiber diameter shows successful coating of nanofibers with chitosan.

3.3. Characterization

The FTIR spectra of neat PVA/SA ENM and CS-f-PVA/SA ENM are shown in Fig. 2a. The spectrum of neat SA/PVA ENM shows IR bands at 3435 cm□ 1, 2945 cm□ 1, 1718 cm□ 1, 1625 cm□ 1 that are assigned to the –OH, CH3, -COOH, and C– – C stretching vibration due to the presence of -COOH and -OH groups in SA, and OH, C– – C and CH3 groups in PVA (due to the presence of non-hydrolyzed vinyl acetate groups). The spectrum of CS-f-SA/PVA ENM also shows similar IR bands but also extra IR bands at 1402 cm□ 1 and 848 cm□ 1, which are related to the CH-OH groups and out-of-plane bending of NH2 of chitosan. It also can be noticed that the intensity of COOH of SA IR band at 1730 cm□ 1 decreased in the spectrum of the CS-f-SA/PVA ENM because of the coating of the SA/PVA nanofibers with chitosan. Besides, the loading content of CS on CS-f-PVA/SA ENM surface was 13.8% in mass measured by the ICP-MS [32]. The thermal degradation behavior of the pristine PVA/SA and CS-f- PVA/SA ENMs was illustrated by thermogravimetric analysis (TGA) shown in Fig. 2b. The pristine PVA/SA ENM exhibited two-stage weight loss. At the first stage between 30 ºC to 95 ºC approx. 4% weight loss occurred due to the loss of moisture absorbed by the composite nanofibers. In the second/final stage, another 84% weight loss was occurred for PVA/SA ENM between 285 ºC to 450 ºC due to the degradation of PVA and SA. On the other hand, the CS-f-PVA/SA ENM showed three-stage degradation. At the first stage, 4.2% weight loss occurred due to the loss of moisture absorbed by the CS-f-PVA/SA ENM. At the second stage between 220 and 350 ◦C, the weight loss (approx. 66%) occurred due to the decomposition of functional groups of PVA, SA, and CS. At the final stage, another 22% weight loss occurred due to the partial degradation of PVA and SA. The addition of CS to PVA/SA reduced the thermal stability of PVA/SA-ENM as the maximum degradation temperatures well as the yield decreased. Fig. 2c illustrates the XRD patterns of PVA/SA and CS-f-PVA/SA ENMs. The XRD patterns of PVA/SA and CS-f-PVA/SA ENMs showed a broad peak at 18–22◦, suggesting that the produced nanofibers were amorphous, which occurred due to the strong intra- and intermolecular hydrogen bonding [40,41]. Fig. 2d, shows that the static water contact angle of neat PVA/SA ENM, which is 62.42 ± 1.5◦ but for the CS-f-PVA/SA ENM the static water contact angle reduced to 31.56 ± 1.7º indicating that the hydrophilicity of the SA/PVA ENM increased after coating with chitosan. Although both ENMs showed hydrophilicity, the surface of CS-f-SA/PVA ENM was considerably more hydrophilic than the surface of neat SA/ PVA ENM due to the coating with hydrophilic chitosan.

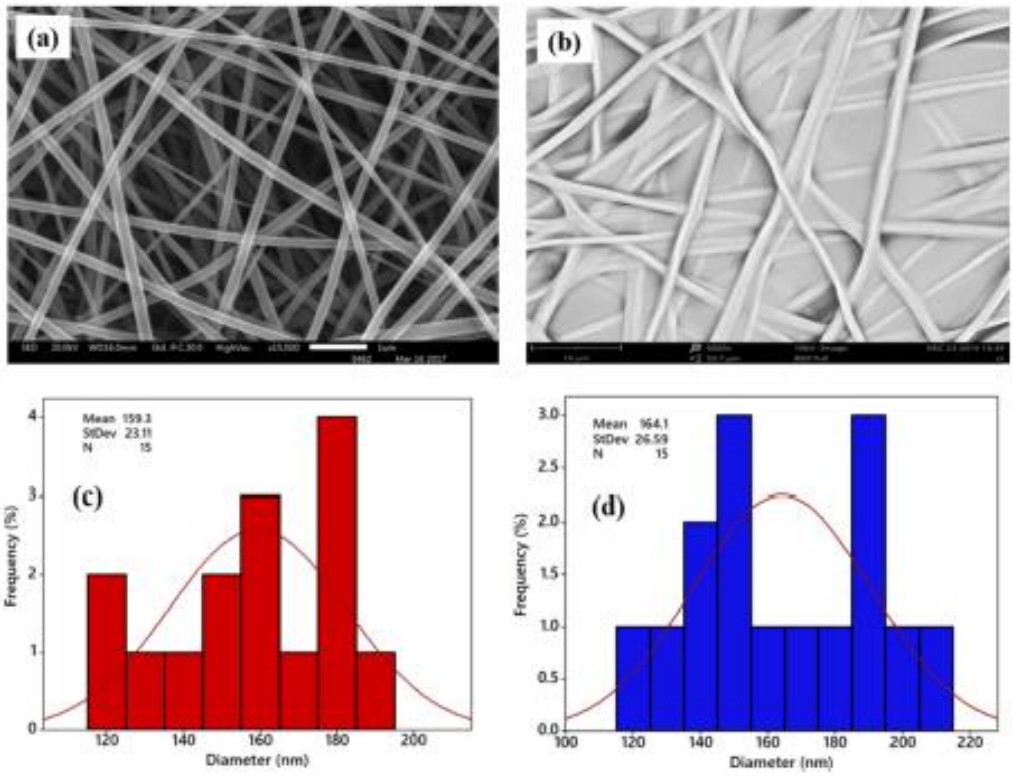

Fig. 1. *SEM and diameter distribution of pristine PVA/SA ENM (a,c), and CS-f-PVA/SA ENM (b,d).*

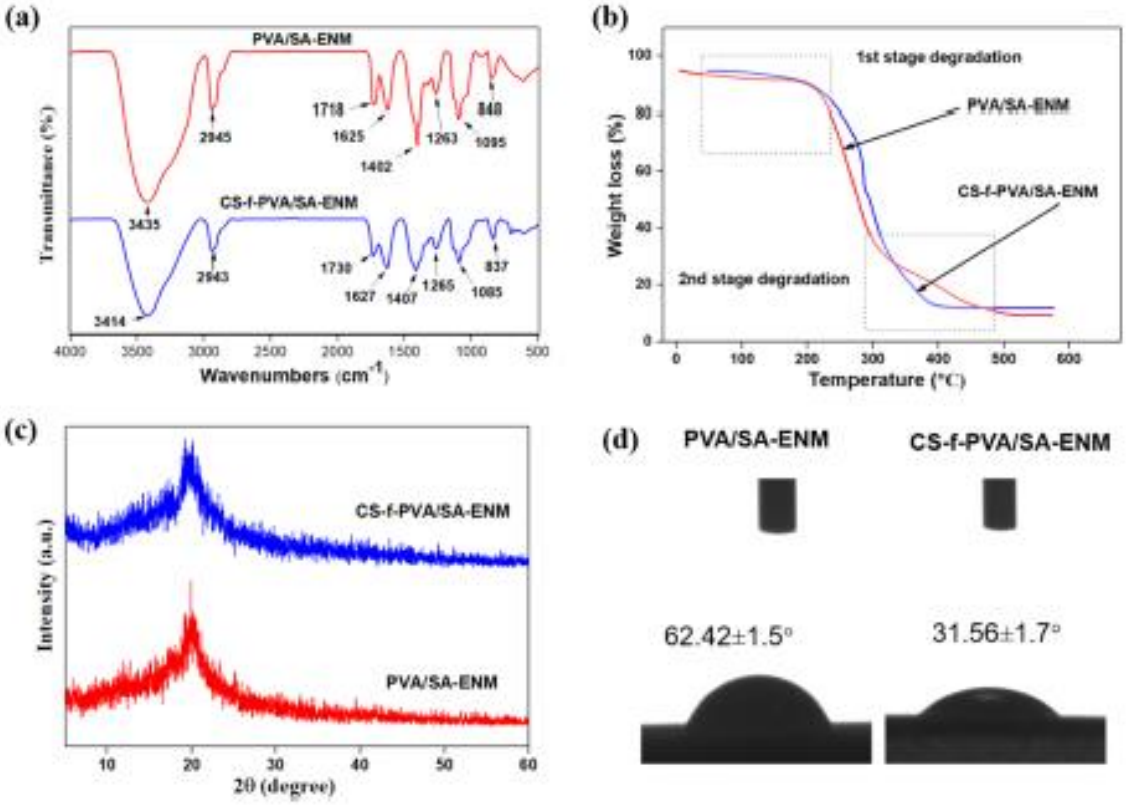

Fig. 2. *FTIR spectra (a), TGA curves (b), XRD pattern (c), and (d) water contact angle of PVA/SA ENM and CS-f-PVA/SA ENM, respectively.*

3.4. As(III) adsorption studies

The effect of dosage rate, contact time, the effect of pH, and initial concentrations on the adsorption of As(III) by SA/PVA and CS-f-SA/PVA was examined. The adsorption kinetics and isotherms were also studied to understand the transfer rate of As(III) from the aqueous solution to the solid ENMs. Additionally, qualitative EDX spectra were employed to analyze the surface elements on the PVA/SA and CS-f-PVA/SA-ENM nanofiber after the As(III) loaded, as shown in Figs. S2a, 1b. EDX result demonstrates that the presence of As(III) in the CS-f-PVA/SA ENM as the elemental composition of As was 12.22%. After of modification of PVA/SA ENM surface with CS, the cationic surface charge increased resulting in an increase in adsorption of As (III) by CS-f-PVA/SA ENM [42,43]. Fig. S3 shows that after the adsorption of As(III) by CS-f-PVA/SA ENM), the diameter of the nanofibers considerably increased (Fig. S3 in Supplementary Materials).

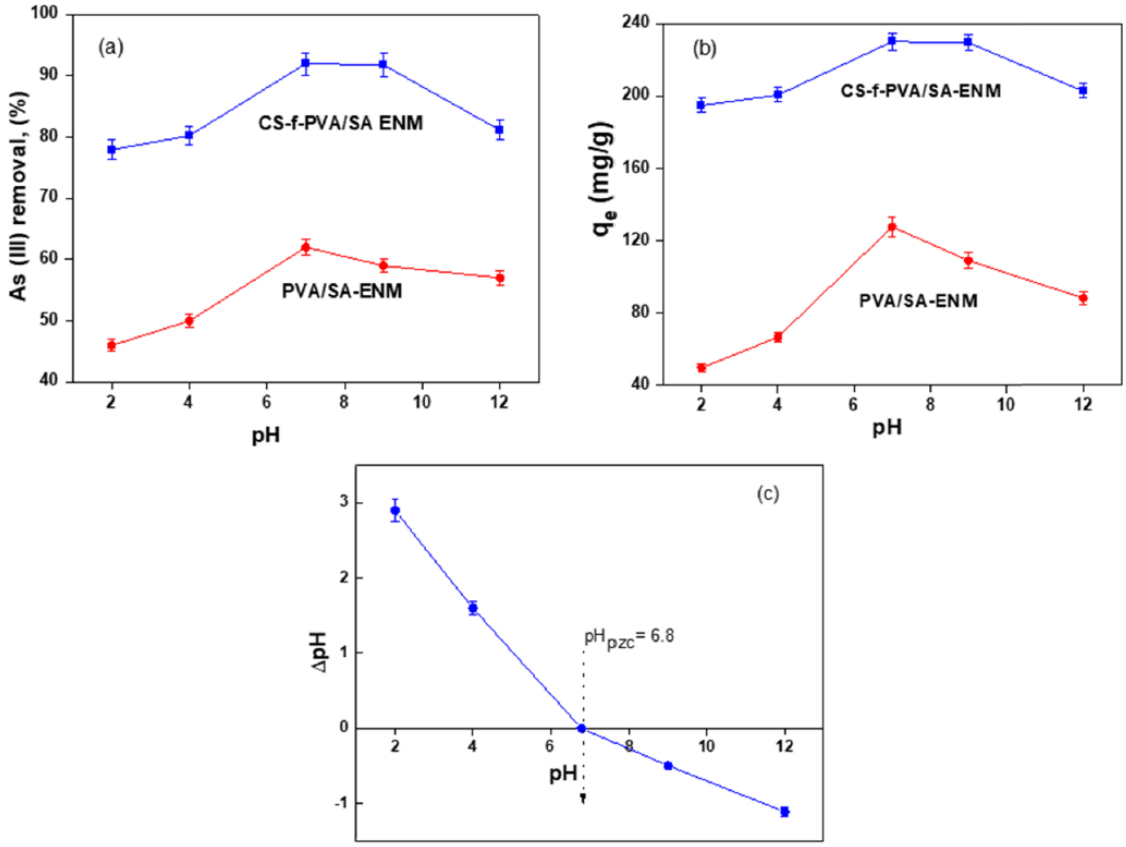

Fig. 3. *Effect of pH on the As(III) removal percentage (a) and adsorption capacity (b) of pristine PVA/SA-ENM and CS-f-PVA/SA ENM and (c) pHpzc plot of CS-f-PVA/ SA ENM.*

3.4.1. Effect of pH on adsorption capacity

The effect of solution pH on As(III) removal rate and adsorption capacities of pristine PVA/SA and CS-f-PVA/SA ENMs are shown in Fig. 3. The change in solution pH changes the adsorbent/adsorbate surface charge, and therefore the solution pH plays an important role in the adsorption behavior. The pristine PVA/SA and CS-f-PVA/SA ENMs both showed the

highest As(III) adsorption capacity at pH 6.5–7.5. Further decrease or increase in solution pH reduced the removal of As for both ENMs, which is consistent with the results reported in published literature [44,45]. At a pH range of 6.5–7.5, the As(III) removal capacity of CS-f-PVA/SA ENM was 90% to 93% with adsorption capacities between 227 and 229 mg g□ 1, whereas for the pristine PVA/SA ENM, te As (III) removal capacity was only 58–62% As(III) with adsorption capacities between 123.4 and 127.6 mg g□ 1. The CS-f-PVA/SA ENM exhibited much higher As(III) binding capacity compared to the PVA/SA ENM. Thus, the CS-f-PVA/SA ENM can be considered as a highly efficient adsorbent for removing As(III) at neutral pH. At neutral pH, the maximum electrostatic interaction occurred between the adsorbent's positively charged amino groups and negatively charged As(III) [46,47]. Besides, the electrostatic attraction and complexation have occurred between hydroxyl group and As(III) [39,48]. The pH effect behavior could be explained in terms of pHpzc of the adsorbent in the solution (pHpzc= 6.8, Fig. 3c), as As(III) adsorption would be facilitated by electrostatic interaction between negatively charged As(III) species ($H_2AsO_3^-$ and $HAsO_3^-$ are predominant in the experimental pH range) and positively charged absorbent surface. In this case, the higher removal efficiency was due to the abundant protonation of the adsorption sites on CS-f-PVA/SA ENM, which interacted with negatively charged arsenate species at pH <pHpzc. With the increasing pH, the net surface charge on the adsorbent became less positive and even negative, and repulsive forces between anionic adsorbate and adsorbent resulted in a decrease of the As(III) adsorption capacity [37, 49].

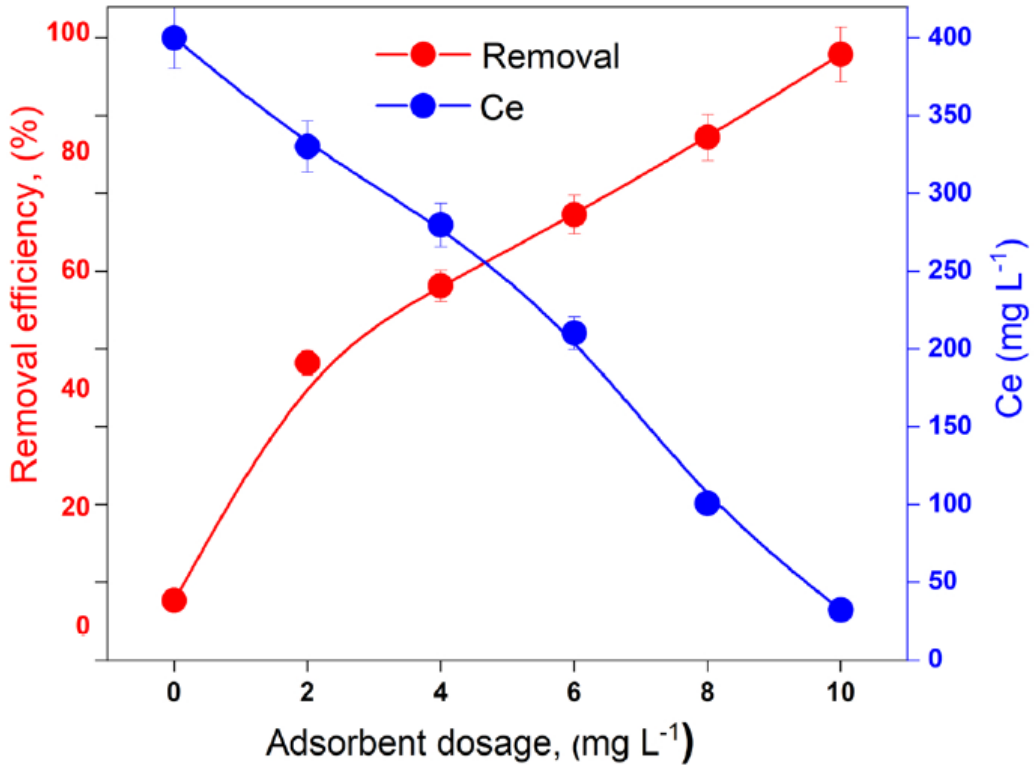

Fig. 4. *Effect of adsorbent dosage on the As(III) removal and its concentration by CS-f-PVA/SA ENM; [As(III)]0 = 0.2 mg L□ 1, initial neutral pH, 220 rpm for 3.5 h, at room temperature.*

3.4.2. Effect of adsorbent dosage

The effect of different adsorbent dosages on the removal of As(III) from its 200 µg L□ 1 aqueous solution is shown in Fig. 4. The concentration of As(III) in the solution rapidly decreased and As(III) removal efficiency increased with an increase in the ENM dosage. For 2 mg L□ 1 adsorbent, the removal efficiency of As(III) was 45% which increased to almost 93% when the applied dosage of CS-f-PVA/SA ENM was increased to 10 mg L□ 1. The adsorption capacity increased from 170 mg g□ 1 to 367 mg g□ 1 with an increase in the dosage of adsorbent from 2 mg L□ 1 to 10 mg L□ 1. This finding indicates that CS-f-PVA/SA ENM demonstrated satisfactory performance for the removal of As (III). As 10 mg L□ 1 adsorbent dosage provided the highest removal of As (III), 10 mg L□ 1 dosage was adopted in the later experiments.

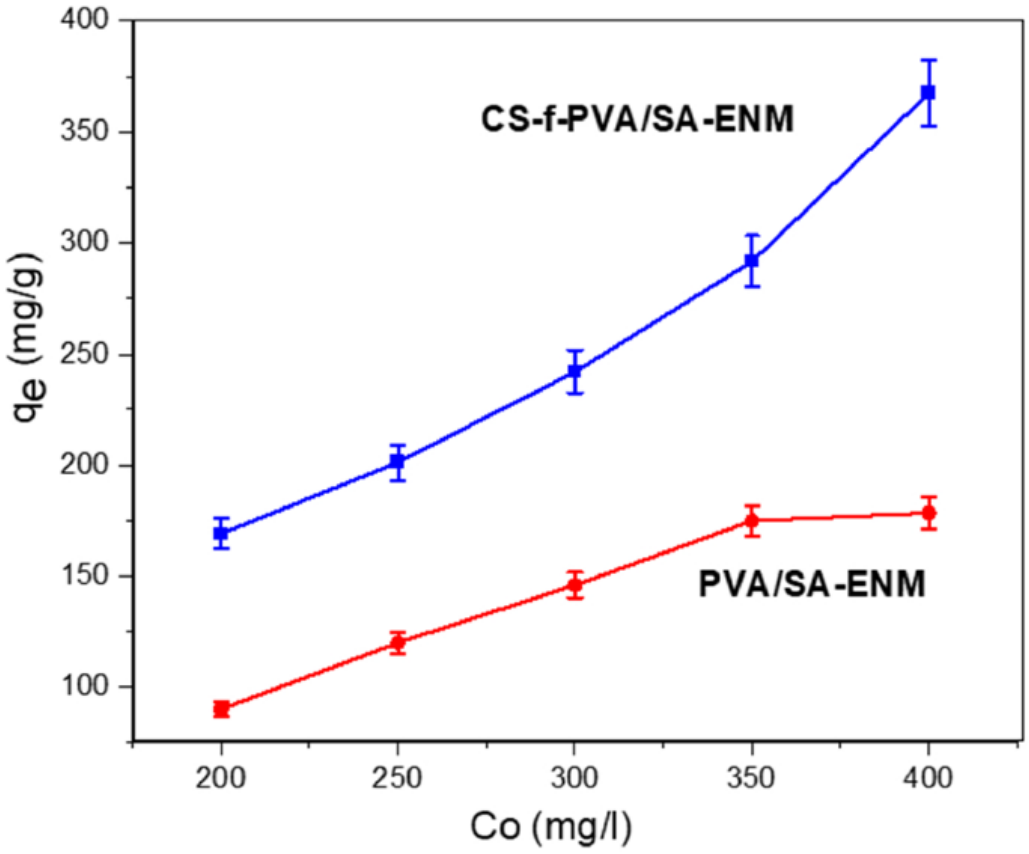

Fig. 5. *The As(III) adsorption capacity of PVA/SA-ENM and (b) CS-f-PVA/ SA ENM.*

3.4.3. Effect of initial concentration

The effect of the initial concentration of As(III) ions on the As binding capacities of the pristine PVA/SA and CS-f-PVA/SA ENMs is shown in Fig. 5. For CS-f-PVA/SA ENM, adsorption capacity rapidly increased with an increase in initial concentration of As(III), whereas, for PVA/SA ENM, it was saturated with As at Csubs0 of 350 mg L□ 1 as at this level the adsorption reached a plateau but for CS-f-PVA/SA ENM, the As(III) binding capacity was still increasing. The CS-f-PVA/SA ENM exhibited the highest adsorption capacity of 367.99 mg

g□ 1 compared to the pristine PVA/SA ENM‘s 178.543 mg g□ 1 As binding capacity at the initial concentration of 400 ug mL□ 1. The addition of cationic CS to PVA/SA considerably enhanced their As(III) binding capacity.

Table 1
Analysis of adsorption kinetics by non-linear Pseudo-first order and Pseudo-second order for CS-f-PVA/SA ENM.

Sample	Pseudo-first-order					Pseudo-second-order				
	Qe (mgg^{-1})	K_1 (min^{-1})	R^2	R^2_{adj}	ARE (%)	Qe (mgg^{-1})	K_2 ($g\ mg^{-1}min^{-1}$)	R^2	R^2_{adj}	ARE (%)
PVA/SA-ENM	166.83	0.023	0.95	0.94	9.5	207.55	0.00013	0.97	0.97	2.8
CS-f-PVA/SA ENM	292.26	0.030	0.94	0.92	9.1	343.80	0.00013	0.98	0.98	2.7

3.4.4. Adsorption kinetics

Adsorption kinetics study play a crucial role in understanding adsorption behavior. In this study, the kinetic behavior of pristine PVA/ SA and CS-f-PVA/SA ENMs were evaluated employing kinetic capacity curves (qt) as a function of contact time (t) for different initial As(III) concentrations (Fig. 6). The adsorption experiments were carried out over 3.5 h at room temperature and natural pH. For CS-f-PVA/SA ENM, the adsorption process progressed rapidly and almost reached equilibrium within 90 min. On the other hand, for the pristine PVA/SA ENM, the adsorption equilibrium reached within 108 min. The adsorption capacities increased gradually regardless the As(III) concentration [34, 37]. More than 90% of the total adsorption of As(III) occurred within the first 60 min for CS-f-PVA/SA ENM, which was much higher than pristine PVA/SA-ENM. The mechanism of As(III) elimination was investigated using the PFO, PSO kinetic models. Sorption is preceded by diffusion across a boundary layer in the PFO model [42]. Chemical surface adsorption, where the removal of adsorbate from a solution is due to chemical interactions between the adsorbent and the adsorbate, is the rate-limiting step in the PSO model [42]. To analyze the adsorption kinetics precisely, PFO (Eq. 3) and PSO (Eq. 4) models were used, which can be expressed as follows:

$Qt = Qe(1 - e^{-k1t})$ *(3)*

$Qt = \frac{k1Qe^2t}{1 + k2Qet}$ (4)

Where Qt (mg g □ 1) and Qe (mg g □ 1) are the adsorption capacity at any time and adsorption equilibrium, the parameters k1 (min □ 1) and k2 (g mg □ 1 min □ 1) are the first and second-order kinetic rate constants, respectively. The adsorption kinetics were fitted by non-linear PFO and PSO models and the relative fitting curves are shown in Fig. 6. In addition, the corresponding kinetics data are summarized in Table 1. For CS-f- PVA/SA ENM, a slightly higher correlation co-efficiency was observed for the PSO (R2 = 0.98) than the PFO (R2 =0.93), as shown in Table 1. On the other hand, for PVA/SA-ENM, the lower correlation co-efficiency was observed for the PFO (R2 =0.94) than the PSO (R2 =0.97), shown in Table 1. The above discussion suggests that the As(III) adsorption onto CS-f-PVA/SA and PVA/SA-ENMs followed PSO kinetics. The chemisorption was occurred during As(III) adsorption onto the CS-f-PVA/SA ENM involving the specific interactions with the surface functional group [50]. The PSO was found to be the most appropriate for describing the kinetic behavior, with the highest value for the coefficient of determination R2 and adjusted coefficient of

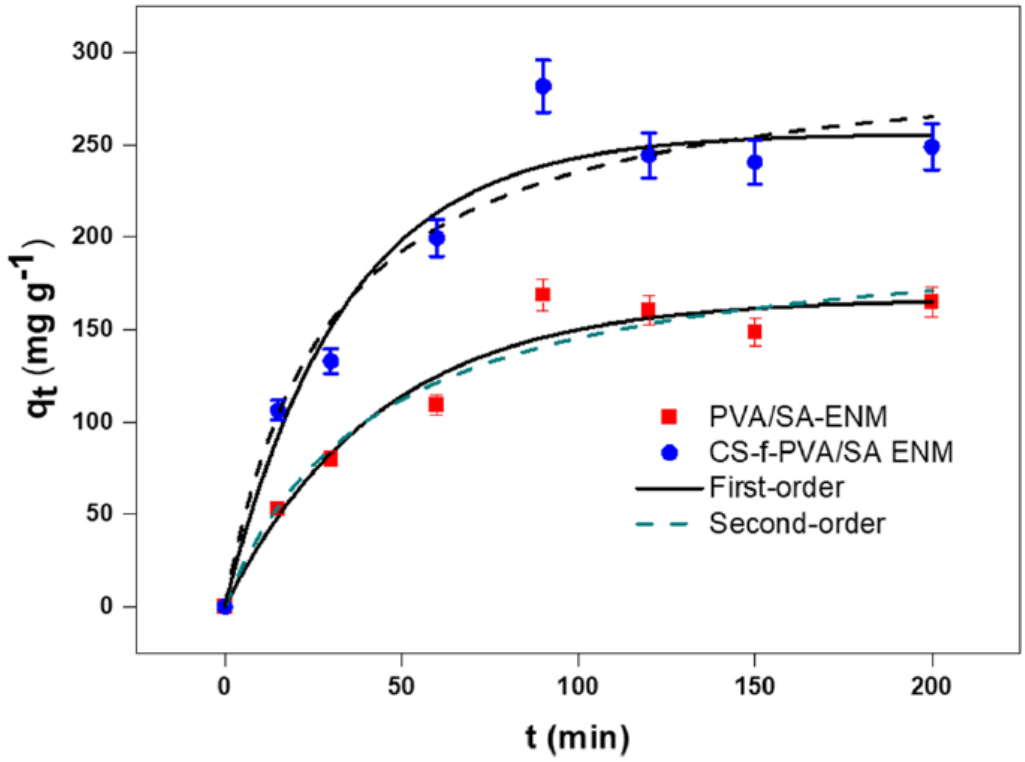

Fig. 6. *Kinetic curves onto CS-f-PVA/SA and PVA/SA ENMs; [As(III)]0 = 0.2 mg L□ 1, at neutral pH, 220 rpm for 3.5 h, at room temperature. (Adjustment of pseudo-first-order and - pseudo-second-order kinetic models to the experimental data).*

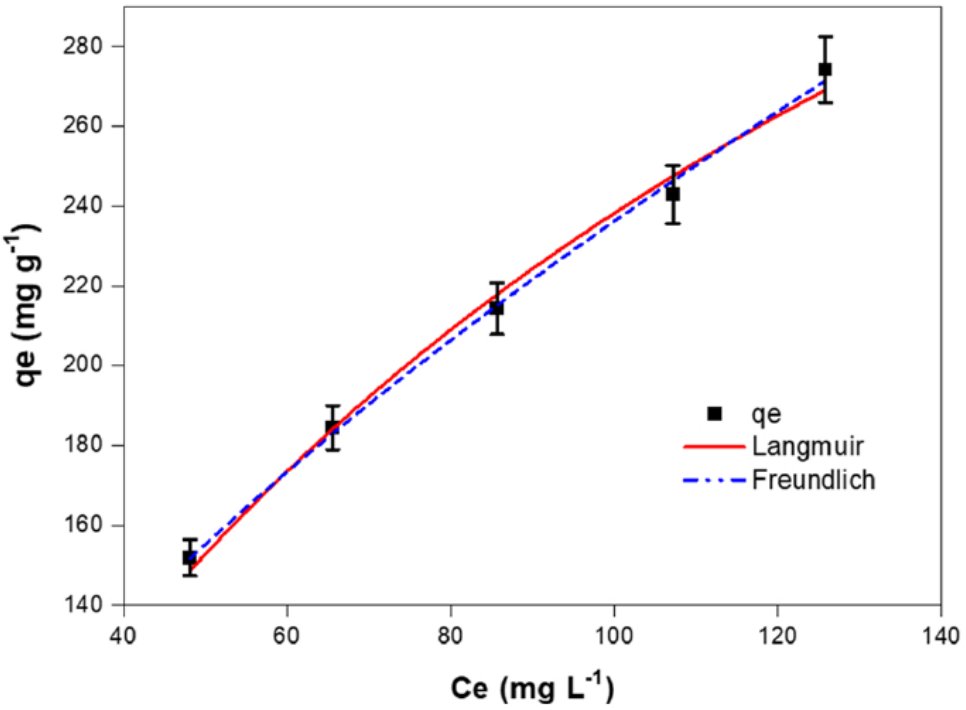

Fig. 7. Equilibrium curves (a) Adsorption isotherm, (b) Langmuir and (c) Freundlich isotherm model for As(III) adsorption onto CS-f-PVA/SA ENM. [As (III)]0 = 0.2 mg L□ 1, initial pH = 7, 3.5 h, and room temperature.

determination (R2adj) (between 0.98 and 0.98) and lowest values for the average relative error (ARE < 2.7%). The PSO model indicates that the adsorption mechanism is dependent on the diffusion-controlled system [49,51]. The maximum adsorption capacities for CS-f-PVA/SA and PVA/SA ENMs were 343.8 mg g□ 1 and 207.82 mg g□ 1, respectively. These results confirm that the chitosan coating (CS-f-PVA/SA ENM) has significantly improved PVA/SA ENM's As(III) adsorption performance.

Table 2
Parameters of Langmuir and Freundlich models for As(III) adsorption isotherm on CS-f-PVA/SA ENM.

	Langmuir					Freundlich				
	Q_{max} (mg/g)	k_L (L mg^{-1})	R^2	R^2_{adj}	ARE (%)	K	1/n	R^2	R^2_{adj}	ARE (%)
As(III)	540.54	0.0079	0.98	0.97	1.4	14.59	0.6047	0.99	0.99	1.2

3.4.5. Adsorption isotherms of As(III)

Many adsorption isotherm models are used for understanding solid-liquid interface adsorption but Langmuir and Freundlich are the most commonly used models [52]. The As(III) adsorption isotherms for CS-f-PVA/SA ENM, are shown in Fig. 7. The CS-s-PVA/SA ENM showed a maximum adsorption capacity of 540.54 mg g□ 1 at neutral pH. It demonstrates that the CS-f-PVA/SA ENM showed considerably higher As(III) adsorption capacity at neutral pH. Adsorption isotherms As(III) is known to all, Langmuir (Eq. 5) and Freundlich (Eq. 6) isotherm models were used to analyze the adsorption equilibriums data, which can be expressed as follows: Qe = *QmkLCe* 1 + *kLCe* (5) Qe = kFCe1/n (6) Where Ce (mg L□ 1) and Qe (mg g□ 1) are the amounts of the equilibrium concentration and equilibrium adsorption quantities, and kF (mg g□ 1) * (L mg□ 1)^1/n is Freundlich constant, and 1/n is the heterogeneity factor. The adsorption isotherm constant was analyzed by the widely used non-linear Langmuir and Freundlich isotherm models. Freundlich isotherm model represents multilayer adsorption, and the Langmuir model represents monolayer adsorption. As shown in Table 2, after analyzing the adsorption data, the correlation coefficients (R2), R2adj and ARE (%) values indicated that the Freundlich model was well fitted and showed a higher regression co-efficiency value than

Table 3
Maximum As(III) adsorption capacity (mg g^{-1}) was reported in the literature from the Isotherm study.

Adsorbent	Max [As]0 (mg L^{-1})	T (°C)	Equilibrium Time (h)	pH	*q*max (mg g-1)	Ref.
CS beads	10	25	24	7	1.94	[53]
CS flakes	2	20	9	4	4.02	[41]
CS flakes	10	24	0.5	4.7	14.2	[54]
zero-valent iron loaded CS nanofiber	25	25	1	6	2.28	[55]
CS	0.5	20	1.8	5	0.5	[56]
CS/PVA nanofiber	10	RT	4	7	0.56	[57]
CS-ENM	133	Rt	0.5	4.4	30.8	[58]
CS-f-PVA/SA ENM	400	RT	1.5	6–7	540.54	This work

the Langmuir model. As(III) adsorption on CS-f-PVA/SA ENM fitted better by the Freundlich isotherm model, indicating a multilayer adsorption mechanism and heterogeneous surface.

Table 3 shows a comparison of As(III) adsorption performance of CS-f-PVA/SA ENM with other CS-based adsorbents. The comparative results show that the CS-f-PVA/SA ENM had excellent adsorption performance, which might be attributed to its surface being rich with amino groups. As (III) was captured by amino groups through electrostatic attraction, which greatly enhanced its removal. Therefore, the surface-modified PVA/SA ENM could be a promising powerful adsorbent for the removal of As(III) from an aqueous solution.

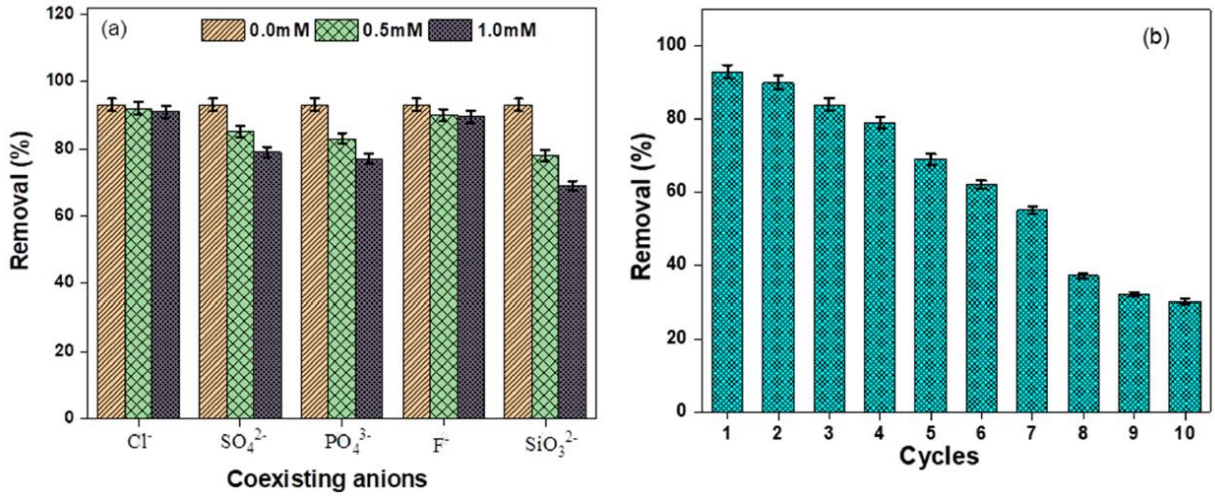

Fig. 8. *(a) Effect of coexistence ions on As(III) removal by CS-f-PVA/SA ENM (b) Regeneration of CS-f-PVA/SA ENM over ten adsorption-desorption cycles with 0.003 M NaOH.*

3.5. Effect of coexisting anions

Here, the effect of coexisting anions on the adsorption of As(III) by the CS-f-PVA/SA ENM adsorbent was examined. There are ubiquitous anions present in polluted water and nature which can affect the As(III) removal, thus reducing the As(III) removal efficiency due to the competitive binding or blocking the adsorbent sites by anions and As (III). In this study, different coexisting representative anions such as Cl□ , SO42□ , SiO32□ , F- and PO43□ with the 0.5 mM and 1.0 mM initial concentration were used. The presence of various competing anions influenced the adsorption capacity and removal of As(III). The effect of co-anions on the As adsorption by CS-f-PVA/SA was examined using the initial concentration of As(III), 0.004 mM, at neutral pH and the results are presented in Fig. 8a. The experimental results indicated that Cl□ and F ions up to 0.5 mM and 1.0 mM concentration didn't show a negative effect on As(III) adsorption, whereas SO42□ , and PO43□ exhibited some levels of negative effects on As(III) adsorption, which is consistent with the As adsorption by similar adsorbents [58–60]. The reasons for the different behavior of coexisting anions were due to different pKa values of the coexisting anions. P and As(III) both have similar chemical speciation [61] which may be a reason for the decrease in the removal efficiency and adsorption capacity [60,62]. A negative influence has occurred for SiO32□ because of steric effects on the surface potential of absorbent with As(III) [60]. Overall, the competitive coexisting anions.

3.6. Regeneration

The developed adsorbent needs to be regenerable and reusable to compete with the commercial adsorbents and these properties are considered as the most crucial indicator to show the performance of an adsorbent. It is usually not easy to desorb the As(III) from adsorbent in an aqueous solution by using 0.1 M concentration NaOH [40]. As shown in Fig. 8b, CS-f-PVA/SA ENM showed highly efficient reusability performance with above 30% of As(III) removal efficiency even after ten times successive cycles, and no change was found in the color, size, weight, and shape of the CS-f-PVA/SA ENM. *3.7. Adsorption mechanism* The removal of As(III) by the one-dimensional (1D) ENM occurred possibly by complexation, and electrostatic interaction adsorption process, as shown in Fig. 9. The hydrogen from the protonation of amino groups and methyl groups of strongly cationic CS-f-PVA/SA ENM was replaced by anionic arsenite utilizing at the low acidic or neutral pH, and similar interaction was observed by Sharma et.al. [63]. The surface-active OH groups of CS-f-PVA/SA ENM may further bind or release As, where the surface remains positive ue to the below Reaction 1: CS-OH + H3O+ = CS-OH2 + H2O Reaction 1 Reaction 1 indicates that the removal efficiency of CS-f-PVA/SA ENM is more at low acidic or neutral pH. In this condition, As(III) adsorption mechanism was represented in two different mechanisms, which were (a) electrostatic interaction between CS-f-PVA/SA ENM positively charged amino groups and negatively charged of As(III) oxoanions (Reaction 2) and (b) electrostatic interaction and complexation between CS-f-PVA/SA ENM surface positively charged of the hydroxyl group and arsenite (Reaction 3) [64]. The dependent pH (range 6.5–7.5) behavior could be explained by the more ionization adsorption of both adsorbent and adsorbate causing the change of electrostatic interaction force. It has been demonstrated that H2AsO3 are the dominant Arsenite species at pH values < 9.0 [65]. CS-NH2 + H2AsO3- = CS-NH2+ - HAsO3- Reaction 2 CS-OH + H3O+ + HAsO3- = CS-NH2+ - HASO3- + H2O Reaction 3

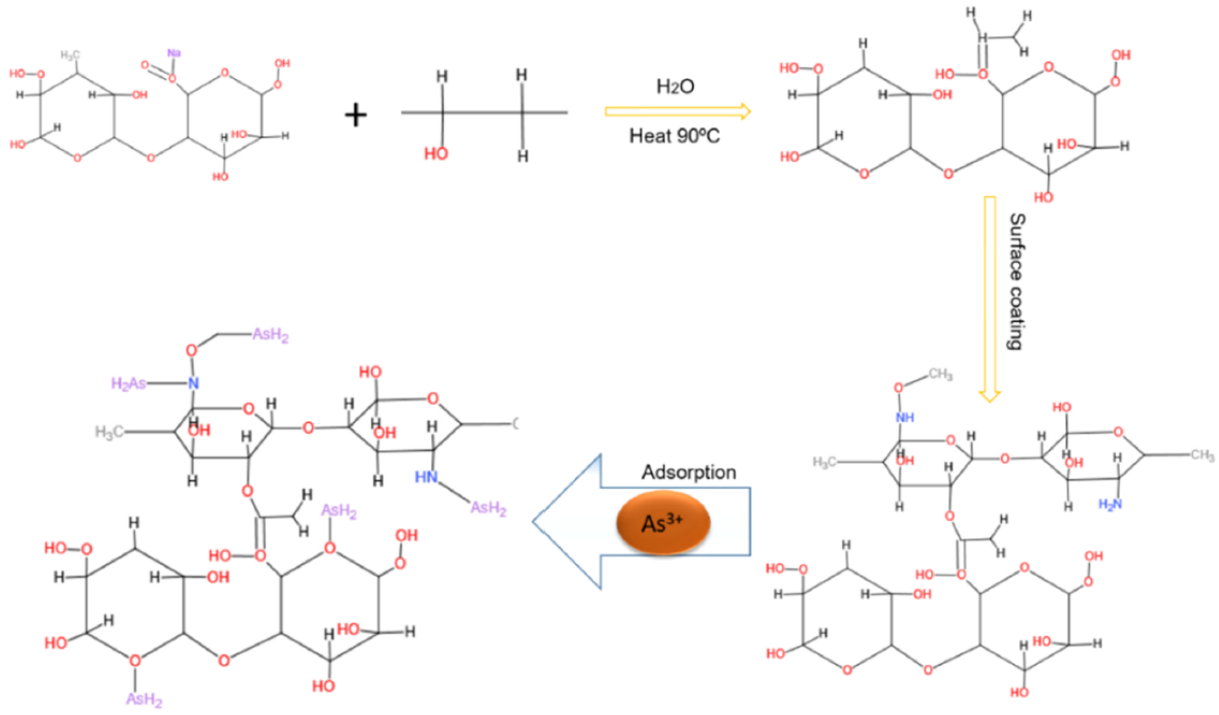

Fig. 9. Proposed adsorption mechanism of As (III) in the presence of CS-f-PVA/SA ENM.

4. Conclusions

We successfully prepared an ENM composed of beads-free nanofibers from CS-f-PVA/SA, which showed considerably higher As(III) binding capacity compared to the pristine PVA/SA ENM. The morphological characterizations carried out by XRD, SEM, TGA, and EDX show that the produced nanofibers are amorphous but fairly uniform in diameter. Based on the experimental results and the kinetics study, the CS-f-PVA/ SA ENM showed the maximum As(III) adsorption capacity (more than 92%) at neutral pH. Compared with PVA/SA ENM, CS-f-PVA/SA ENM demonstrated exceptionally higher As(III) adsorption capacity. The adsorption equilibrium reached within 90 min and the adsorption kinetic is well fitted with the pseudo-second-order kinetics model than the pseudo-first-order kinetics model. The CS-f-PVA/SA ENM exhibited a maximum absorption capacity up to 540.54 mg g□ 1 and the adsorption isotherm is well-fitted with the Freundlich isothermal model. Additionally, the spectroscopic analysis implied that –NH2, –OH, and C–O could make the dominant contributions for the As(III) adsorption onto CS-f-PVA/SA ENM. The presence of coexisting anions of Cl□ and F- up to 1.0 mM didn't cause a negative effect on the As(III) adsorption, whereas SO42□ slightly affected the As adsorption at 1.0 mM, but SiO32□ and PO43□ greatly interfered the sorption of As onto CS-f-PVA/SA ENM surface. The recycle and reusability of CS-f-PVA/SA ENM was studied with 0.003 M NaOH, and the As adsorption performance was still 80% after 4 times recycle and reuse. This study demonstrates that the developed ENM can be used for the removal of As(III) from potable water and can be a potential green adsorbent for the trace level of As(III) removal from water with high adsorption capacity and easy separation from water.

CRediT authorship contribution statement

Md Eman Talukder, **Md. Nahid Pervez**, **Wang Jianming**: Experimental investigation, Data analysis, Methodology, Writing – original draft. **Md Eman Talukder**, **Md. Nahid Pervez**, **Wang Jianming**, **Ziwei Gao**: Experimental investigation, Data analysis, Characterization. **Md. Nahid Pervez**, **George K Stylios**, **Mohammad Mahbubul Hassan**: Writing – review & editing. **Hongchen Song**, **Vincenzo Naddeo**: Conceptualization, Funding acquisition, Project administration, Supervision, Writing – review & editing. **Declaration of Competing Interest** The authors declare that they have no known competing financial interests or personal relationships that could have appeared to influence the work reported in this paper.

Acknowledgments

This work was supported by the Shenzhen Institute of Advanced Technology, the Chinese Academy of Sciences, Shenzhen, China. The authors are also grateful to the Shenzhen Institute of Advanced Technology, the Chinese Academy of Sciences, Shenzhen, China. This research work was funded by Shenzhen Science and Technology program (grant number: KCXFZ 2021221173402006). In addition, we would like to express our sincere gratitude for the support from the Sanitary Environmental Engineering Division (SEED) and grants (FARB projects) from the University of Salerno, Italy, coordinated by prof. V. Naddeo. The PhD School in "Risk and Sustainability in Civil Engineering, Environmental and Construction" is also acknowledged for the scholarships (cycle-XXXIV) of M.N. Pervez.

References

[1] A.P. Singh, R.K. Goel, T. Kaur, Mechanisms pertaining to arsenic toxicity, Toxicol. Int. 18 (2011) 87, https://doi.org/10.4103/0971-6580.84258.

[2] D.K. Nordstrom, Worldwide occurrences of arsenic in ground water, Science 296 (2002) 2143–2145, https://doi.org/10.1126/science.1072375.

[3] M.N. Pervez, Y. Wei, P. Sun, G. Qu, V. Naddeo, Y. Zhao, α-FeOOH quantum dots impregnated graphene oxide hybrids enhanced arsenic adsorption: the mediation role of environmental organic ligands, Sci. Total. Environ. 781 (2021), 146726, https://doi.org/10.1016/j.scitotenv.2021.146726.

[4] Q. Zheng, J. Hou, W. Hartley, L. Ren, M. Wang, S. Tu, W. Tan, As (III) adsorption on Fe-Mn binary oxides: are Fe and Mn oxides synergistic or antagonistic for arsenic removal? Chem. Eng. J. 389 (2020), 124470 https://doi.org/10.1016/j. cej.2020.124470.

[5] M.N. Pervez, D. Fu, X. Wang, Q. Bao, T. Yu, V. Naddeo, H. Tian, C. Cao, Y. Zhao, A bifunctional α-FeOOH@GCA nanocomposite for enhanced adsorption of arsenic and photo Fenton-like catalytic conversion of As(III), Environ. Technol. Innov. 22 (2021) 101437.

[6] S. Alka, S. Shahir, N. Ibrahim, M.J. Ndejiko, D.-V.N. Vo, F. Abd Manan, Arsenic removal technologies and future trends: a mini review, J. Clean. Prod. 278 (2021), 123805, https://doi.org/10.1016/j.jclepro.2020.123805.

[7] M.N. Pervez, G.K. Stylios, An experimental approach to the synthesis and optimisation of a ‘green’ nanofibre, Nanomaterials 8 (2018) 383, https://doi.org/ 10.3390/nano8060383.

[8] M.E. Talukder, K.M.F. Hasan, J. Wang, J. Yao, C. Li, H. Song, Novel fibrin functionalized multilayered electrospun nanofiber membrane for burn wound treatment, J. Mater. Sci. 56 (2021) 12814–12834, https://doi.org/10.1007/ s10853-021-06123-6.

[9] X. Wang, B.S. Hsiao, Electrospun nanofiber membranes, Curr. Opin. Chem. 12 (2016) 62–81, https://doi.org/10.1016/j.coche.2016.03.001.

[10] M.N. Pervez, M. Balakrishnan, S.W. Hasan, K.-H. Choo, Y. Zhao, Y. Cai, T. Zarra, V. Belgiorno, V. Naddeo, A critical review on nanomaterials membrane bioreactor (NMs-MBR) for wastewater treatment, npj Clean Water 3 (2020) 43, https://doi. org/10.1038/s41545-020-00090-2.

[11] S. Moon, B.-Y. Ryu, J. Choi, B. Jo, R.J. Farris, The morphology and mechanical properties of sodium alginate based electrospun poly(ethylene oxide) nanofibers, Polym. Eng. Sci. 49 (2009) 52–59, https://doi.org/10.1002/pen.21216.

[12] Q. Xiao, L.-T. Lim, Pullulan-alginate fibers produced using free surface electrospinning, Int. J. Biol. Macromol. 112 (2018) 809–817, https://doi.org/ 10.1016/j.ijbiomac.2018.02.005.

[13] W. Li, X. Li, Y. Chen, X. Li, H. Deng, T. Wang, R. Huang, G. Fan, Poly(vinyl alcohol)/sodium alginate/layered silicate based nanofibrous mats for bacterial inhibition, Carbohydr. Polym. 92 (2013) 2232–2238, https://doi.org/10.1016/j. carbpol.2012.12.004.

[14] M.N. Pervez, G.K. Stylios, Y. Liang, F. Ouyang, Y. Cai, Low-temperature synthesis of novel polyvinylalcohol (PVA) nanofibrous membranes for catalytic dye degradation, J. Clean. Prod. 262 (2020), 121301, https://doi.org/10.1016/j. jclepro.2020.121301.

[15] S. Safi, M. Morshed, S.A. Hosseini Ravandi, M. Ghiaci, Study of electrospinning of sodium alginate, blended solutions of sodium alginate/poly(vinyl alcohol) and sodium alginate/poly(ethylene oxide), J. Appl. Polym. Sci. 104 (2007) 3245–3255, https://doi.org/10.1002/app.25696.

[16] Q. Wang, J. Ju, Y. Tan, L. Hao, Y. Ma, Y. Wu, H. Zhang, Y. Xia, K. Sui, Controlled synthesis of sodium alginate electrospun nanofiber membranes for multi-occasion adsorption and separation of methylene blue, Carbohydr. Polym. 205 (2019) 125–134, https://doi.org/10.1016/j.carbpol.2018.10.023.

[17] M. Wang, X. Li, T. Zhang, L. Deng, P. Li, X. Wang, B.S. Hsiao, Eco-friendly poly (acrylic acid)-sodium alginate nanofibrous hydrogel: a multifunctional platform for superior removal of Cu(II) and sustainable catalytic applications, Colloids Surf. A Physicochem. Eng. Asp. 558 (2018) 228–241, https://doi.org/10.1016/j. colsurfa.2018.08.074.

[18] T.C. Mokhena, N.V. Jacobs, A. Luyt, Electrospun alginate nanofibres as potential bio-sorption agent of heavy metals in water treatment, eXPRESS Polym. Lett. 11 (2017) 652–663, https://doi.org/10.3144/expresspolymlett.2017.63.

[19] F. Ebrahimi, A. Sadeghizadeh, F. Neysan, M. Heydari, Fabrication of nanofibers using sodium alginate and Poly(Vinyl alcohol) for the removal of Cd2+ ions from aqueous solutions: adsorption mechanism, kinetics and thermodynamics, Heliyon 5 (2019), e02941, https://doi.org/10.1016/j.heliyon.2019.e02941.

[20] J. Ma, L. Zhong, X. Peng, Y. Xu, R. Sun, Functional chitosan-based materials for biological applications, Curr. Med. Chem. 27 (2020) 4660–4672, https://doi.org/ 10.2174/0929867327666200420091312.

[21] M.N. Pervez, G.K. Stylios, Investigating the synthesis and characterization of a novel “green” H2O2-assisted, water-soluble chitosan/polyvinyl alcohol nanofiber for environmental end uses, Nanomaterials 8 (2018) 395, https://doi.org/ 10.3390/nano8060395.

[22] X. Pang, M. Bouzid, J.M.N. dos Santos, Mh Gazzah, G.L. Dotto, H. Belmabrouk, A. Bajahzar, A. Erto, Z. Li, Theoretical study of indigotine blue dye adsorption on CoFe2O4/chitosan magnetic composite via analytical model, Colloids Surf. A Physicochem. Eng. Asp. 589 (2020), 124467, https://doi.org/10.1016/j. colsurfa.2020.124467.

[23] J.O. Gonçalves, K.A. da Silva, E.C. Rios, M.M. Crispim, G.L. Dotto, L.A. de Almeida Pinto, Chitosan hydrogel scaffold modified with carbon nanotubes and its application for food dyes removal in single and binary aqueous systems, Int. J. Biol. Macromol. 142 (2020) 85–93, https://doi.org/10.1016/j.ijbiomac.2019.09.074.

[24] J. Desbri`eres, E. Guibal, Chitosan for wastewater treatment, Polym. Int. 67 (2018) 7–14, https://doi.org/10.1002/pi.5464.

[25] R. Vidal, J. Moraes, Removal of organic pollutants from wastewater using chitosan: a literature review, Int. J. Environ. Sci. Technol. 16 (2019) 1741–1754, https:// doi.org/10.1007/s13762-018-2061-8.

[26] V.V.L. Carvalho, J.O. Gonçalves, A. Silva, T.R. Cadaval, L.A.A. Pinto, T.J. Lopes, Separation of anthocyanins extracted from red cabbage by adsorption onto chitosan films, Int. J. Biol. Macromol. 131 (2019) 905–911, https://doi.org/ 10.1016/j.ijbiomac.2019.03.145.

[27] X. Zhao, S. Chen, Z. Lin, C. Du, Reactive electrospinning of composite nanofibers of carboxymethyl chitosan cross-linked by alginate dialdehyde with the aid of polyethylene oxide, Carbohydr. Polym. 148 (2016) 98–106, https://doi.org/ 10.1016/j.carbpol.2016.04.051.

[28] Y. Hu, Z. Zhang, Y. Li, X. Ding, D. Li, C. Shen, F.-J. Xu, Dual-crosslinked amorphous polysaccharide hydrogels based on chitosan/alginate for wound healing applications, Macromol. Rapid. Commun. 39 (2018), 1800069, https://doi.org/ 10.1002/marc.201800069.

[29] J.H. Chen, J.C. Ni, Q.L. Liu, S.X. Li, Adsorption behavior of Cd (II) ions on humic acid-immobilized sodium alginate and hydroxyl ethyl cellulose blending porous composite membrane adsorbent, Desalination 285 (2012) 54–61, https://doi.org/ 10.1016/j.desal.2011.09.033.

[30] M.S. Islam, M.R. Karim, Fabrication and characterization of poly (vinyl alcohol)/ alginate blend nanofibers by electrospinning method, Colloids Surf. A Physicochem. Eng. Asp. 366 (2010) 135–140, https://doi.org/10.1016/j. colsurfa.2010.05.038.

[31] F. Ebrahimi, A. Sadeghizadeh, F. Neysan, M. Heydari, Fabrication of nanofibers using sodium alginate and Poly (Vinyl alcohol) for the removal of Cd2+ ions from aqueous solutions: adsorption mechanism, kinetics and thermodynamics, Heliyon 5 (2019), e02941.

[32] L. Qi, Z. Xu, Lead sorption from aqueous solutions on chitosan nanoparticles, Colloids Surf. A Physicochem. Eng. Asp. 251 (2004) 183–190, https://doi.org/ 10.1016/j.colsurfa.2004.10.010.

[33] Z. Zhao, J. Zheng, M. Wang, H. Zhang, C.C. Han, High performance ultrafiltration membrane based on modified chitosan coating and electrospun nanofibrous PVDF scaffolds, J. Membr. Sci. 394 (2012) 209–217, https://doi.org/10.1016/j. memsci.2011.12.043.

[34] L.N. Cˆortes, S.P. Druzian, A.F.M. Streit, M. Godinho, D. Perondi, G.C. Collazzo, M. L.S. Oliveira, T.R.S. Cadaval Jr, G.L. Dotto, Biochars from animal wastes as alternative materials to treat colored effluents containing basic red 9, J. Environ. Chem. Eng. 7 (2019), 103446, https://doi.org/10.1016/j.jece.2019.103446.

[35] G.L. Dotto, T.R.S. Cadaval, L.A.A. Pinto, Use of Spirulina platensis micro and nanoparticles for the removal synthetic dyes from aqueous solutions by biosorption, Process Biochem. 47 (2012) 1335–1343, https://doi.org/10.1016/j. procbio.2012.04.029.

[36] A.C. Fr¨ohlich, E.L. Foletto, G.L. Dotto, Preparation and characterization of NiFe2O4/activated carbon composite as potential magnetic adsorbent for removal of ibuprofen and ketoprofen pharmaceuticals from aqueous solutions, J. Clean. Prod. 229 (2019) 828–837, https://doi.org/10.1016/j.jclepro.2019.05.037.

[37] L.L. Min, L.B. Zhong, Y.M. Zheng, Q. Liu, Z.H. Yuan, L.M. Yang, Functionalized chitosan electrospun nanofiber for effective removal of trace arsenate from water, Sci. Rep. 6 (2016) 32480, https://doi.org/10.1038/srep32480.

[38] D. Malwal, P. Gopinath, Rapid and efficient removal of arsenic from water using electrospun CuO–ZnO composite nanofibers, RSC Adv. (2016) 115021–115028, https://doi.org/10.1039/C6RA24023B.

[39] F. Amiri, M.M. Rahman, H. B¨ornick, E. Worch, Sorption behaviour of phenols on natural sandy aquifer material during flow-through column experiments: the effect of pH, Acta Hydrochim. Hydrobiol. 32 (2004) 214–224, https://doi.org/10.1002/ aheh.200300531.

[40] V.M. Boddu, K. Abburi, J.L. Talbott, E.D. Smith, R. Haasch, Removal of arsenic (III) and arsenic (V) from aqueous medium using chitosan-coated biosorbent, Water Res. 42 (2008) 633–642, https://doi.org/10.1016/j.watres.2007.08.014.

[41] C. Gerente, Y. Andres, G. Mckay, P. Le Cloirec, Removal of arsenic (V) onto chitosan: from sorption mechanism explanation to dynamic water treatment process, Chem. Eng. J. 158 (2010) 593–598, https://doi.org/10.1016/j. cej.2010.02.005.

[42] N. Najib, C. Christodoulatos, Removal of arsenic using functionalized cellulose nanofibrils from aqueous solutions, J. Hazard. Mater. 367 (2019) 256–266, https://doi.org/10.1016/j.jhazmat.2018.12.067.

[43] R. Roque-Malherbe, R.C.D.L.P. del, Synthesis characterization, and adsorption properties of nanoporous materials. Appl. Surf. Sci., IntechOpen, 2019, https://doi. org/10.5772/intechopen.83355.

[44] S.R. Kanel, B. Manning, L. Charlet, H. Choi, Removal of arsenic (III) from groundwater by nanoscale zero-valent iron, Environ. Sci. Technol. 39 (2005) 1291–1298, https://doi.org/10.1021/es048991u.

[45] S. Bhowmick, S. Chakraborty, P. Mondal, W. Van Renterghem, S. Van den Berghe, G. Roman-Ross, M. Iglesias, Montmorillonite-supported nanoscale zero-valent iron for removal of arsenic from aqueous solution: Kinetics and mechanism, Chem. Eng. J. 243 (2014) 14–23, https://doi.org/10.1016/j.cej.2013.12.049.

[46] J.S. Yamani, A.W. Lounsbury, J.B. Zimmerman, Adsorption of selenite and selenate by nanocrystalline aluminum oxide, neat and impregnated in chitosan beads, Water Res. 50 (2014) 373–381, https://doi.org/10.1016/j.watres.2013.10.054.

[47] A.B. Giasuddin, S.R. Kanel, H. Choi, Adsorption of humic acid onto nanoscale zerovalent iron and its effect on arsenic removal, Environ. Sci. Technol. 41 (2007) 2022–2027, https://doi.org/10.1021/es0616534.

[48] S. Mandal, M.K. Sahu, R.K. Patel, Adsorption studies of arsenic (III) removal from water by zirconium polyacrylamide hybrid material (ZrPACM-43), Water Resour. Ind. 4 (2013) 51–67, https://doi.org/10.1016/j.wri.2013.09.003.

[49] M.S. Netto, J.S. Oliveira, N.P. Salau, G.L. Dotto, Analysis of adsorption isotherms of Ag+, Co+ 2, and Cu+ 2 onto zeolites using computational intelligence models, J. Environ. Chem. Eng. 9 (2021), 104960, https://doi.org/10.1016/j. jece.2020.104960.

[50] L.D.O. Yamil, J. Georgin, D.S. Franco, M.S. Netto, D.G. Piccilli, E.L. Foletto, L. F. Oliveira, G.L. Dotto, High-performance removal of 2, 4-dichlorophenoxyacetic acid herbicide in water using activated carbon derived from Queen palm fruit endocarp (Syagrus romanzoffiana), J. Environ. Chem. Eng. 9 (2021), 104911, https://doi.org/10.1016/j.jece.2020.104911.

[51] J. Georgin, D.S. Franco, M.S. Netto, D. Allasia, E.L. Foletto, L.F. Oliveira, G. L. Dotto, Transforming shrub waste into a high-efficiency adsorbent: application of Physalis peruvian chalice treated with strong acid to remove the 2, 4-dichlorophenoxyacetic acid herbicide, J. Environ. Chem. Eng. 9 (2021), 104574, https:// doi.org/10.1016/j.jece.2020.104574.

[52] A.O. Dada, A.P. Olalekan, A.M. Olatunya, O.J.I.J.C. Dada, Langmuir, Freundlich, Temkin and Dubinin–Radushkevich isotherms studies of equilibrium sorption of Zn2+ unto phosphoric acid modified rice husk, IOSR J. Appl. Chem. 3 (2012) 38-45.

[53] C.C. Chen, Y.C. Chung, Arsenic removal using a biopolymer chitosan sorbent, J. Environ. Sci. Health A 41 (2006) 645–658, https://doi.org/10.1080/ 10934520600575044.

[54] K.C. Kwok, V.K. Lee, C. Gerente, G. McKay, Novel model development for sorption of arsenate on chitosan, Chem. Eng. J. 151 (2009) 122–133, https://doi.org/ 10.1016/j.cej.2009.02.004.

[55] N. Horzum, M.M. Demir, M. Nairat, T. Shahwan, Chitosan fiber-supported zero-valent iron nanoparticles as a novel sorbent for sequestration of inorganic arsenic, RSC. Adv (2013) 7828–7837, https://doi.org/10.1039/C3RA23454A.

[56] B.M. Min, S.W. Lee, J.N. Lim, Y. You, T.S. Lee, P.H. Kang, W.H. Park, Chitin and chitosan nanofibers: electrospinning of chitin and deacetylation of chitin nanofibers, Polymer 45 (2004) 7137–7142, https://doi.org/10.1016/j. polymer.2004.08.048.

[57] D. Chauhan, J. Dwivedi, N. Sankararamakrishnan, Novel chitosan/PVA/zerovalent iron biopolymeric nanofibers with enhanced arsenic removal applications, Environ. Sci. Pollut. Res. 21 (2014), https://doi.org/10.1007/s11356-014-2864-1, 9430-7442.

[58] L.L. Min, Z.H. Yuan, L.B. Zhong, Q. Liu, R.X. Wu, Y.M. Zheng, Preparation of chitosan based electrospun nanofiber membrane and its adsorptive removal of arsenate from aqueous solution, Chem. Eng. J. 267 (2015) 132–141, https://doi. org/10.1016/j.cej.2014.12.024.

[59] G. Zhang, J. Qu, H. Liu, R. Liu, R. Wu, Preparation and evaluation of a novel Fe–Mn binary oxide adsorbent for effective arsenite removal, Water Res. 41 (2007) 1921–1928, https://doi.org/10.1016/j.watres.2007.02.009.

[60] T. Tuutij¨arvi, E. Repo, R. Vahala, M. Sillanp¨a¨a, G. Chen, Effect of competing anions on arsenate adsorption onto maghemite nanoparticles, Chin. J. Chem. Eng. 20 (2012) 505–514, https://doi.org/10.1016/S1004-9541(11)60212-7.

[61] Y. Ma, Y.M. Zheng, J.P. Chen, A zirconium based nanoparticle for significantly enhanced adsorption of arsenate: synthesis, characterization and performance, J. Colloid Interface Sci. 354 (2011), https://doi.org/10.1016/j.jcis.2010.10.041.

[62] H. Cui, Q. Li, S. Gao, J.K. Shang, Strong adsorption of arsenic species by amorphous zirconium oxide nanoparticles, J. Ind. Eng. Chem. 18 (2012) 1418–1427, https:// doi.org/10.1016/j.jiec.2012.01.045.

[63] R. Sharma, N. Singh, A. Gupta, S. Tiwari, S.K. Tiwari, S.R. Dhakate, Electrospun chitosan–polyvinyl alcohol composite nanofibers loaded with cerium for efficient removal of arsenic from contaminated water, J. Mater. Chem. A 2 (2014) 16669–16677, https://doi.org/10.1039/C4TA02363C.

[64] M. LL, Y. LM, W. RX, Z. LB, Y. ZH, Z. YM, Enhanced adsorption of arsenite from aqueous solution by an iron-doped electrospun chitosan nanofiber mat: Preparation, characterization and performance. J. Colloid. Interface. Sci. 535, 2019, 255–264. https://doi.org/10.1016/j.jcis.2018.09.073.

[65] B. S, C. S, M. P, V.R. W, V.d.B. S, R.-R. G, C. D, I. M, Montmorillonite-supported nanoscale zero-valent iron for removal of arsenic from aqueous solution: Kinetics and mechanism. Chem. Eng. J. 243 (2014) 14–23.